ChemSusChem

Research Article
doi.org/10.1002/cssc.202300296

Chemistry Europe
European Chemical Societies Publishing

www.chemsuschem.org

Organic Redox Targeting Flow Battery Utilizing a Hydrophilic Polymer and Its In-Operando Characterization via State-of-Charge Monitoring of The Redox Mediator

Erik Schröter,[a, b] Christian Stolze,[a, b] Jakob Meyer,[a, b] Martin D. Hager,[a, b] and Ulrich S. Schubert*[a, b]

The hydrophilic poly(2,2,6,6-tetramethylpiperdinyloxy-4-yl-methacrylamide) (PTMAm) was utilized as redox target material in an aqueous organic redox targeting flow battery (RTFB). This polymer is processed into granules, which contain a conductive agent and an alginate binder. By this, a hydrophilic, yet water-insoluble redox target can be obtained. The target was combined with the redox mediator molecule *N*,*N*,*N*-trimethyl-2-oxo-2-[(2,2,6,6-tetramethylpiperidin-4-yloxyl)amino]ethan-1-ammonium chloride (TEMPOAmide), that has been reported earlier as flow battery active material. This target/mediator combination has been characterized electrochemically and flow battery testing has been done. Furthermore, in-operando characterization of the redox target via electrolyte state-of-charge (SOC) monitoring has been performed for the first time. The approach provides estimates for the redox target's SOC changes during cycling. In addition, a figure of merit – the "redox targetivity" – is proposed, which provides insights into the efficiency of the targeting reaction and supports the future optimization of materials, cell designs, and operational parameters for RTFBs.

Introduction

Redox flow batteries have been subject to research in the field of sustainable energy storage technologies for 50 years.[1] As stationary storage devices, they represent a promising alternative to lithium-based technologies and established large-scale energy storages.[1] While vanadium and bromine based technologies have been commercialized and can be purchased for home photovoltaic plants as well as peak load shaving in commercial application scenarios, many other inorganic flow batteries suffer from major drawbacks such as necessary aggressive electrolytes and toxic active materials.[1,2] Also, mainly vanadium-based redox flow batteries (RFBs) are in competition for resources to the constantly increasing steel industry and are subject to strong price fluctuations.[3] As a consequence, organic flow batteries show a high potential as future alternative.[1,4] However, all of the conventional flow battery systems cannot compete with the solid inorganic batteries when it comes to volumetric energy density, as the capacity of the electrolytes is strongly limited by the solubility of the redox-active materials in the utilized solvents. Approaches to overcome this drawback involve suspension-based flow batteries, redox active electrolyte solvents, and, more recently, redox targeting.[5] The latter approach involves the combination of a solid redox active material, the redox target (RT), and at least one dissolved redox mediator (RM). Here, the RM solution is used to charge a solid redox polymer that is stored within the electrolyte storage containers. First organic redox targeting approaches relied on (1) multiple RMs with the same redox group as the RT[6] or (2) a single RM and a single RT with distinct redox groups but similar standard potentials.[7,8] We recently presented a third approach, which combines a single RM and a single RT based on the same redox moiety (TEMPO).[9] This approach excels in its design simplicity as well as its potential cost-efficiency, reduces unwanted chemical interactions between the RT and RM, and naturally provides potential-matched mediators and targets. Currently, this approach is getting increasing attention by other researchers in the field.[10,11]

In our former approach, *N*,*N*,*N*,2,2,6,6-heptamethylpiperidin-1-oxyl chloride (TMATEMPO) was utilized as RM and poly(TEMPO-methacrylate) (PTMA) as RT. However, PTMA can be considered as rather hydrophobic. It is, thus, hindering the swelling of the polymer in the aqueous RM solution and, consequently, decreases the rate capability and total capacity. In order to address those challenges, a more hydrophilic amide derivative of the TEMPO redox polymer was considered as RT, namely poly(TEMPO-methacrylamide) (PTMAm).[12] This polymer is a representative for the group of hydrophilic TEMPO redox polymers, which have been pioneered by the Nishide group in 2009.[13] As this chemical modification also leads to a change of the standard potential of the RT, another *N*,*N*,*N*-trimethyl-2-oxo-

[a] *E. Schröter, Dr. C. Stolze, J. Meyer, Dr. M. D. Hager, Prof. Dr. U. S. Schubert*
Laboratory of Organic and Macromolecular Chemistry (IOMC)
Friedrich Schiller University Jena
Humboldtstraße 10, 07743 Jena (Germany)
E-mail: ulrich.schubert@uni-jena.de
Homepage: http://www.schubert-group.uni-jena.de/en

[b] *E. Schröter, Dr. C. Stolze, J. Meyer, Dr. M. D. Hager, Prof. Dr. U. S. Schubert*
Center for Energy and Environmental Chemistry Jena (CEEC Jena)
Friedrich Schiller University Jena
Philosophenweg 7a, 07743 Jena (Germany)
Homepage: http://www.schubert-group.uni-jena.de/en

2-[(2,2,6,6-tetramethylpiperidin-4-yloxyl)amino]ethan-1-ammonium chloride (TEMPOAmide) was investigated as RM, since it was presented earlier as a stable TEMPO-based redox-active material for aqueous organic redox flow batteries.[14] Flow batteries have been constructed and the material combination was evaluated in a fully operating quasi-symmetrical flow battery setup, where the non-capacity limiting side contained a large amount of TMATEMPO-based electrolyte and no RT. Furthermore, a new figure of merit is mathematically derived in this study based on the charge transfer in the flow cell and the state-of-charge (SOC) change of the RM and it is demonstrated that the SOC change of the RT can be inferred from the data. This new parameter – termed the redox targetivity – is used to characterize the redox targeting process in-operando and to unravel the system's specific limitations.

Results and Discussion

Theory

During battery operation, a total amount of charge, $Q(t)$, is stored in the half-cell containing the RM and the RT. A portion of this charge, $Q_{RM}(t)$, charges or discharges the RM, while the remaining part, $Q_{RT}(t)$, is transferred to the RT. At each point in time, charge conservation demands for one half-cell that the total change in stored charge is the sum of the changes in the RM and the RT:

$$\Delta Q(t) = \Delta Q_{RM}(t) + \Delta Q_{RT}(t). \tag{1}$$

The transfer of charge between the RT and RM per unit of time is – in general – a complex function of, for example, the equilibrium potential difference between RM and RT,[9,15] the redox targeting's reaction kinetics,[10,15] the mass transfer of the RM to the RT surface, and the inherent charge propagation within the RT. It is, thus, an implicit function of the charging current applied at the flow cell, the pumping speed, and electrolyte parameters like viscosity and temperature. Due to the inherent system setup required to operate a redox targeting flow battery, it is difficult to monitor the evolution of the charge transfer between the RM and the RT in-operando. However, it is fairly obvious that important insights may be gained from such data if it would be available. In the following sections we propose a new method to address this issue.

Redox target state-of-charge

The absolute SOCs of the RM and the RT can be defined by the initial charge stored in each of the materials, $Q_{RM,0}$ and $Q_{RT,0}$, the additional charge transferred during the charging/discharging process, $\Delta Q_{RT}(t)$ and $\Delta Q_{RM}(t)$, and their total capacity $Q_{RM,t}$ and $Q_{RT,t}$, respectively:

$$SOC_{RM}(t) = Q_{RM,0}Q_{RM,t}^{-1} + \Delta Q_{RM}(t)Q_{RM,t}^{-1} = Q_{RM}(t)Q_{RM,t}^{-1}, \tag{2}$$

$$SOC_{RT}(t) = Q_{RT,0}Q_{RT,t}^{-1} + \Delta Q_{RT}(t)Q_{RT,t}^{-1} = Q_{RT}(t)Q_{RT,t}^{-1}.$$

Considering that it is experimentally difficult to determine the initial state-of-charge of the redox target, it is more convenient to take only the change of the state of charge into account:

$$\Delta SOC_{RM}(t) = \Delta Q_{RM}(t)Q_{RM,t}^{-1}, \tag{3}$$

$$\Delta SOC_{RT}(t) = \Delta Q_{RT}(t)Q_{RT,t}^{-1}$$

Inserting both equations into Equation (1) and rearranging for the state-of-charge change of the redox target, $\Delta SOC_{RT}(t)$, one arrives at:

$$\Delta SOC_{RT}(t) = \frac{\Delta Q(t) - \Delta SOC_{RM}(t)\ Q_{RM,t}}{Q_{RT,t}} \tag{4}$$

This equation enables the estimation of the state-of-charge change of the RT, if the total charge transferred during battery charging/discharging (ΔQ), the state-of-charge change of the redox mediator (ΔSOC_{RM}), and the total capacities of the RM ($Q_{RM,t}$) and the RT ($Q_{RT,t}$) are known. All of these quantities can be measured in-operando or can at least be theoretically estimated. If the initial state-of-charge, $SOC_{RT,0}$, of the redox target is known or can be measured, one may even obtain the absolute state-of-charge, $SOC_{RT}(t) = SOC_{RT,0} + \Delta SOC_{RT}(t)$, of the RT:

$$SOC_{RT}(t) = SOC_{RT,0} + \frac{\Delta Q(t) - \Delta SOC_{RM}(t)\ Q_{RM,t}}{Q_{RT,t}} \tag{5}$$

However, it should be considered that the accuracy of the determined state-of-charge change and the absolute state-of-charge, respectively, is highly dependent on the accuracy of all the other parameters. $\Delta Q(t)$ is readily assessable from the applied or measured current flowing through the flow cell during battery operation, $\Delta SOC_{RM}(t)$ may be accurately measured by various available state-of-charge monitoring methods,[16] and the total capacity of the electrolyte can be determined in potentiostatic flow battery measurements prior to the addition of the RT as demonstrated earlier.[9] However, the capacity of the RT can only be estimated from its composition and the known specific capacities of the redox-active substance.

Redox targetivity

Although the SOC change of the RT can already provide a detailed insight into the in-operando evolution of the redox targeting reaction, a more direct quantification is desirable. We therefore derived a new dimensionless figure of merit, ε_{RT}, that we termed the redox targetivity and which we defined as the ratio of the current used to charge/discharge the RT, i_{RT}, with respect to the total charging/discharging current, i_T:

$$\varepsilon_{RT} = i_{RT} i_T^{-1}. \quad (6)$$

The total current is applied at the flow cell and leads to a direct charging/discharging of the RM. This process is counterbalanced by the charge transferred between the RT and RM in the redox targeting reaction. The overall process can be understood as the simultaneous charging/discharging of the RM with the current i_{RM} and the charging/discharging of the RT with the current i_{RT}:

$$i_T(t) = i_{RM}(t) + i_{RT}(t). \quad (7)$$

Therefore, using Equation (2), the average SOC of the RM can be estimated by:

$$SOC_{RM}(t) = SOC_{RM,0} + Q_{RM,0}^{-1} \int_0^t [i_T(\tau) - i_{RT}(\tau)] d\tau, \quad (8)$$

where $SOC_{RM,0}$ is the initial SOC of the electrolyte. Using both the time derivative of Equation (8) and the defining Equation (6), the redox targetivity can be experimentally estimated by measuring the instantaneous rate of change of the RM's SOC:

$$\varepsilon_{RT} = 1 - \frac{Q_{RM,0}}{i_T} \frac{dSOC_{RM}}{dt} \quad (9)$$

An alternative form, which takes into consideration that the total current is the time derivative of the absolute charge transferred between the half-cell, $i_T = \dot{Q}(t)$, is the following:

$$\varepsilon_{RT} = 1 - Q_{RM,0} \frac{dSOC_{RM}}{dQ} \quad (10)$$

In other words, the redox targetivity can be obtained from the relationship between the SOC and the charge transferred between the two half-cells of the RFB. This quantity could also be suited for a comparison of different targeting systems. However, care should be taken during such comparisons and interpretation of the redox targetivity data in general, since ε_{RT} is dependent on several operational factors as well as material parameters including the packing density of the RT in the tank, its composition, the flow speed of the electrolyte, the applied total current during charging/discharging, the kinetics of the redox targeting reaction, and the concentration as well as the diffusivity of the RM. A first proof-of-principle measurement with this approach is discussed at the end of this study.

Results

Both the TEMPOAmide and the PTMAm investigated as RM and RT in this study, respectively, are available through straight forward lab-scale synthesis.[12,14] They are structurally closely related, as both show an amide bond in the 4-position of the redox-active TEMPO-moiety. In case of the PTMAm, the amide connects the TEMPO to the crosslinked polymer backbone, that mediates the insolubility while maintaining the hydrophilic character of the amide bond. The exact structure of both materials is depicted in Scheme 1.

For the Nernstian potential-driven redox targeting approach, the potential difference between the RM and the RT needs to be minimized in order to maximize the capacity utilization of the target.[7] Furthermore, the potential matching is necessary to obtain equally efficient charging and discharging reactions. In the case of a strong potential mismatch, one of these reactions would be strongly favored, which reduces the overall feasibility of the redox targeting system and results in large voltage losses. The reduction of voltage losses also represents one of the major advantages when compared to redox targeting approaches with two RM's. Consequently, the redox potentials of the RM and the RT of this study were measured via cyclic voltammetry (CV) in a three-electrode setup at different supporting electrolyte concentrations. As for our previously reported system, the potential difference was the lowest in a 1 M $NaCl_{aq}$ solution.[9] Here, a formal redox potential of 641 mV *vs.* Ag/AgCl was obtained for the RM. For the RT, a value of 662 mV *vs.* Ag/AgCl was measured. Consequently, a potential difference of −21 mV was obtained (Figure 1).

To check the suitability of the mediator-target system for the Nernstian potential-driven redox targeting approach qualitatively, a thin-layer CV setup was utilized, that was pioneered by Zhou et al. and adapted by our group to the aqueous approach utilizing TEMPO moieties.[7,9] The setup introduces an absorbent separator, that prevents the inert working electrode from touching a RT containing thin-layer electrode while providing sufficient contact to the RM. This enables the redox targeting process to take place between the RM molecules oxidized/reduced at the working electrode during the CV experiment and the RT. By this process, the solid redox active material can be addressed without direct contact to the working electrode. If a redox targeting takes place, it can be recognized by a change in the shape of the CV signal towards a sigmoidal curve. When the RM is present in the soaked separator, the RM molecules can be oxidized on the working electrode surface and, subsequently, diffuse to the RT, where they are reduced again, charging the redox target.

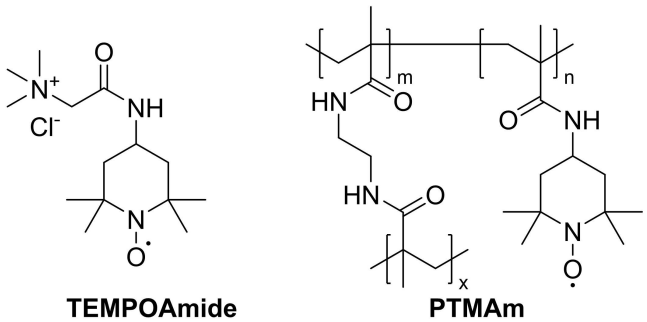

Scheme 1. Schematic representation of the chemical structures of the redox mediator TEMPOAmide and the redox target PTMAm.

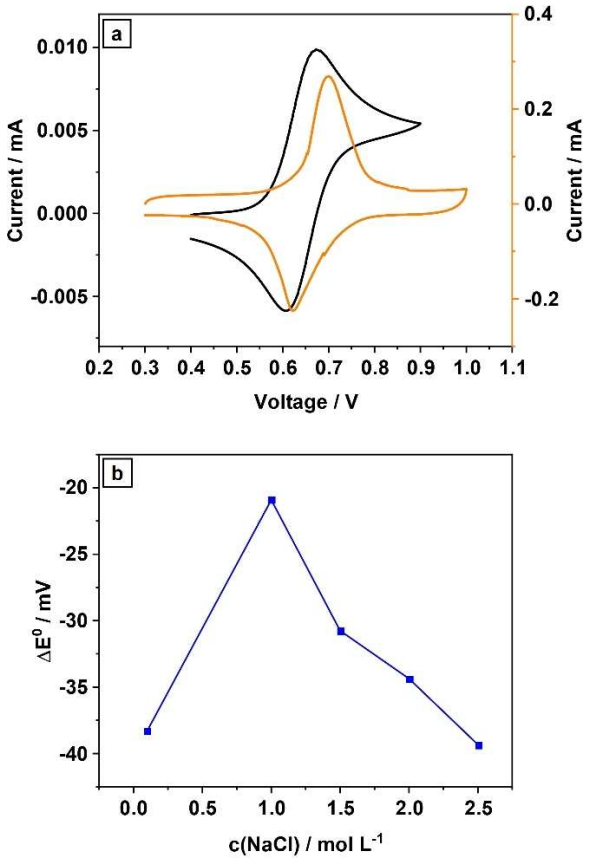

Figure 1. a) Cyclic voltammograms of the redox mediator solution of 10 mM TEMPOAmide in 1 M $NaCl_{aq}$ (black) and PTMAm composite thin-films (orange) at 10 mV s^{-1}. b) Potential difference between the half wave potentials of TEMPOAmide and PTMAm at different NaCl concentrations in aqueous solution.

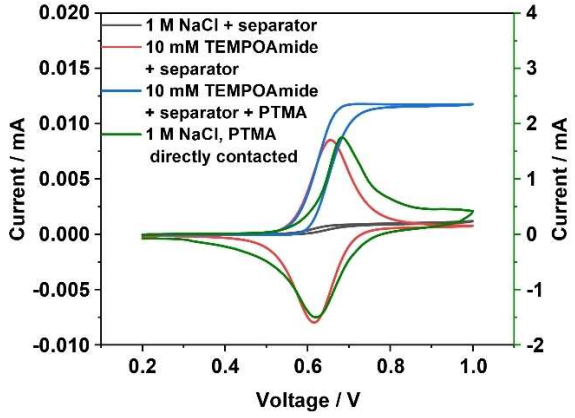

Figure 2. Investigation of redox targeting ability through cyclic voltammetry at 10 mV s^{-1}. The sigmoidal curve (blue) suggests a stationary diffusion profile of the redox mediator molecules between the working electrode and the redox target layer.

This process causes the sharp CV signal to flatten ultimately resulting in a sigmoidal curve shape (Figure 2). The current plateau observed due to this process can be understood as the result of a stationary concentration profile of the RM forming over the separator because of the competing oxidation and reduction processes at the working electrode and the RT, respectively. When the RT is isolated from the working electrode through a supporting electrolyte solution-soaked separator, no CV signal is obtained, as no RM is present on the surface of the electrode. On the other hand, a standard CV signal is observed when a mediator-soaked separator is used and no RT is present. The result of this experiment proves the general suitability of the TEMPOAmide/PTMAm system for the Nernstian redox targeting approach.

For application in the flow battery, the PTMAm had to be transferred into a thin-film battery analogous composite, that is suitable for the flow battery. In our previous work, the RT composite was obtained by mixing the conductive agent, the polymer, and the organic binder in *N*-methyl-2-pyrrolidone (NMP) with subsequent drying and milling.[9] This process was initially repeated for the PTMAm, which was then filled into a flow-through cartridge according for the RFB operation. While the RT capacity was partially addressed, however, the batteries suffered from high pressure and limited pumping ability due to the small particle size of the composite. This is attributed to the swelling behavior of the polymer, which can lead to sedimentation into the pores of the filter in the RT cartridge. Furthermore, the swelling is pronounced in the charged state, which can cause the filter in the cartridge to be fully blocked. In addition, the previous processing towards composite electrode material requires the use of the toxic solvent NMP.

To mitigate these issues, a new aqueous processing route was considered for the hydrophilic PTMAm-carbon composite. Porous granules containing the polymer were prepared from an aqueous slurry by mixing sodium alginate solution with the active material and a conductive agent. A very similar approach for water-processable, but water-insoluble electrode films has been reported by Ding et al. previously.[17] Sodium alginate features the water solubility of the commonly utilized carboxymethylcellulose binders and can be made insoluble through contact with calcium ions. This effect is explained by the formation of "egg-box"-like chelate complexes of the guluronate units of the alginate and calcium ions.[18]

For the slurry, the polymer and conductive agent were swollen in an aqueous sodium alginate solution and homogenized by blade stirring. After drying, an alginate bound composite is obtained, that can be resuspended in water and extruded into an aqueous $CaCl_2$-solution from a syringe. The calcium ions are immediately chelated by the alginate binder, upon which the alginate becomes water insoluble, fixing the polymer and conductive agent in the composite matrix. This effect maintains the insolubility of the composite in water at increased hydrophilicity. The extrudate is subsequently frozen in liquid nitrogen and lyophilized, which resulted in a porous composite material, that could be cut in small, millimeter sized pieces (Figure 3). Afterwards, these granules could be introduced to the battery setup by adding a liquid chromatography cartridge, filled with the composite as in previous approaches.

As first battery experiment, the granular material was introduced into a volumetrically unbalanced, compositionally symmetrical flow battery at 10 mM TEMPOAmide on the

Figure 3. a) Composite material "worms" after extrusion from a syringe into the calcium chloride solution. b) Dried composite material after lyophilization and cutting into smaller particles. c) Scanning electron microscopy image obtained from the extruded and dried composite material. The small circular particles are the conductive agent particles that surround the polymeric active material.

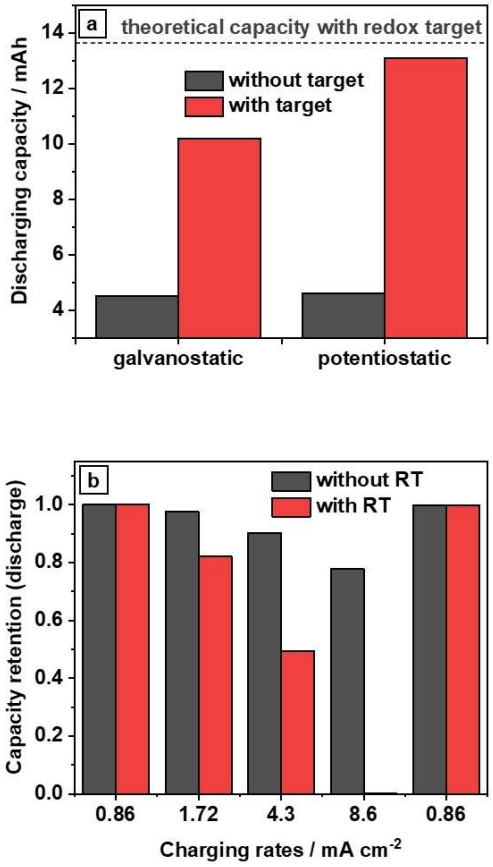

Figure 4. Rate testing experiments of the 10 mM TEMPOAmide batteries in 1 M NaCl solution. a) Addressable discharge capacity for the 10 mM redox flow cells without redox target (grey) and after the addiction of the redox target (red). The values were obtained after galvanostatic cycling at 0.86 mA cm^{-2} or potentiostatic cycling. b) Capacity retention of a redox flow cell before (grey) and after (red) addition of the redox target during cycling at 0.86, 1.72, 4.3, and 8.6 mA cm^{-2}. The charging rate of 17.2 mA cm^{-2} is not displayed, as no capacity was achieved at this rate. The last column represents again cycling at 0.86 mA cm^{-2} to compare the cyclability before and after the rate capability test.

capacity-limiting side according to our previous study.[9] A rate testing experiment (Figure 4) was performed to investigate the RT utilization under different charging/discharging conditions.

By introducing the target material into the system, the capacity of the flow battery can be significantly improved to 226% of the initial value (without RT) for the galvanostatic cycling at 0.86 mA cm^{-2} and to 291% for the potentiostatic charging mode. During the galvanostatic cycling 10.2 mAh (75%) of the theoretically expected 13.6 mAh of capacity were addressed. For the potentiostatic cycling, 13.1 mAh are achieved, which amounts to 96% of the theoretical capacity and highlights the importance of the kinetics for the Nernstian potential-driven redox targeting. In general, the experiments revealed a strong rate dependence for the capacity utilization of the RT. In particular, for current densities higher than 8.6 mA cm^{-2} little to no RT capacity could be addressed in the 10 mM TEMPOAmide batteries, resulting in strongly varying coulombic efficiencies. Also, at 4.3 mA cm^{-2} the addressable RT capacity is already reduced strongly, while the battery still performs the cycles reversibly. This lower rate capability at higher charging rates might be overcome in the future by smaller redox target composite particles of higher porosity and with defined nano- or microstructure. In general, a significant increase of the RT-RM-interface should also lead to a significant increase in the targeting reaction and, thus, facilitate the rate capability.

Furthermore, more sophisticated cartridge designs might strongly influence the wetting of the RT particles with the RM solution. For instance, a fluidized bed-type cartridge can result in improved rate performance as convection is much stronger there compared to the stationary particle layer in the cartridge that has been utilized so far.

Subsequently, the same battery was set up for the long-term cycling experiments (Figure 5). At the low current density of 0.86 mA cm^{-2}, the battery was operated for 100 cycles exhibiting a coulombic efficiency of 99%. In the following experiment (Figure 6), the concentration of the RM was increased from 10 to 100 mM. Accordingly, also the amount of the RT was increased by one order of magnitude to approximately 1.5 g. Overall, the same battery performance could be observed as for the low-concentration redox targeting flow battery. The higher concentration does not appear to change

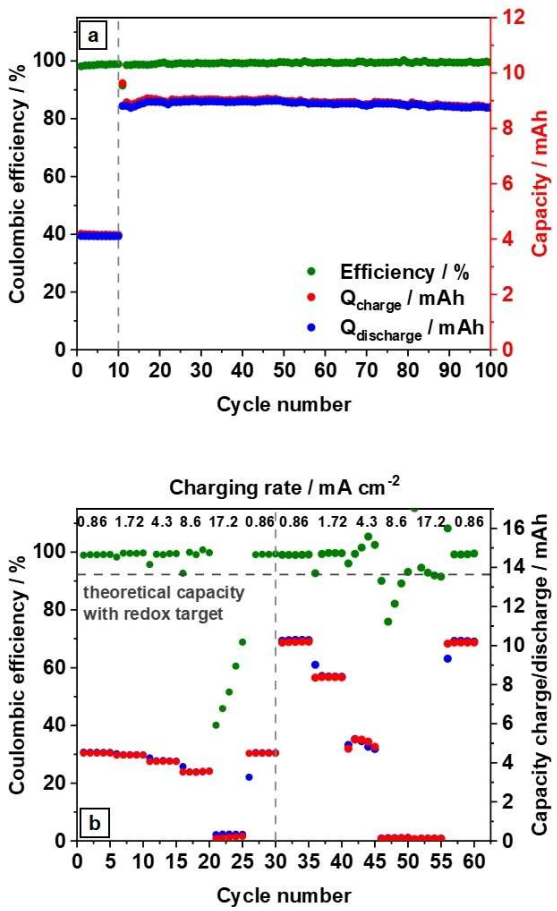

Figure 5. Summary of the long-term cycling experiments over 15 days with a RM concentration of 10 mM before and after the addition of the RT. a) Coulombic efficiency and charge/discharge capacity for cycling the battery at 0.86 mA cm^{-2} for 100 cycles. b) Rate test for the identical cell at 0.86 mA cm^{-2}, 1.72 mA cm^{-2}, 4.3 mA cm^{-2}, 8.6 mA cm^{-2}, and 17.2 mA cm^{-2} before and after (vertical dashed line) the addition of the redox target.

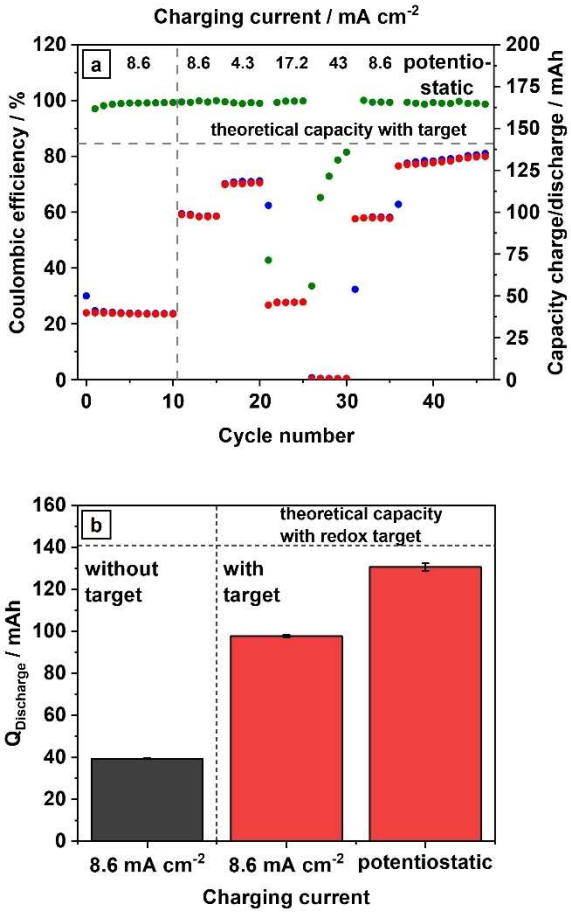

Figure 6. Summary of the flow battery experiments for the redox targeting battery with a RM concentration of 100 mM and a catholyte volume of 16 mL. a) Efficiency, charge and discharge capacities during both galvanostatic cycling (rates given) and potentiostatic cycling. b) Comparison of the achieved discharge capacities for the 100 mM redox targeting battery.

the overall usability of the system and the redox targeting process can be observed to a similar extend as before.

For the galvanostatic cycling at 8.6 mA cm^{-2}, a capacity increase to 248% of the initial capacity was measured. For potentiostatic cycling, an average of 332% of the initial capacity was obtained. Of 141 mAh of theoretical total capacity of the full redox targeting flow battery, approximately 131 mAh (93%) were addressed during the potentiostatic cycling. Less, namely 98 mAh (70%), was addressed when the battery was cycled galvanostatically at 8.6 mA cm^{-2}. Higher charging rates of 17.2 mA cm^{-2} impacted the addressable capacity strongly and reduced it to the level observed initially for the system without RT, which indicates that only the RM capacity was accessed. Finally, no charging capacity could be retained at a rate of 43 mA cm^{-2}.

Despite the limited rate capability, the results clearly demonstrate that the millimeter sized PTMAm composite granules are suitable as RT material irrespective of the RM concentration. The observed capacity utilization of $>$93% is a significant increase compared to our previous TEMPO-based systems that relied on the utilization of finely ground composite powders and the rather hydrophobic PTMA.[9]

At a closer look on the charge/discharge capacities during the potentiostatic cycling, a slight increase in capacities is recognizable. This can be explained by the increased hydrophilicity of charged TEMPO-units that leads to an increased material hydrophilicity and, subsequently, a better wettability of the composite. This facilitates the swelling of the granules and, thus, makes the initially inaccessible redox active sites inside the targeting granules accessible during consecutive cycling.

In a last experiment, the redox targetivity of a 0.1 M TEMPOAmide/1.5 g PTMAm redox targeting flow battery was measured at 4.3 mA cm^{-2} as a first proof-of-principle of this type of analyses (Figure 7). As described in the theoretical section of this study, the SOC change of the RT was inferred from the charge transferred between the half-cells during charging/discharging and the SOC of the RM via Equation (5). The latter was measured with a symmetric open-circuit cell.[19] The total capacity of the electrolyte (51.4 mAh) and the calibration parameters of the open-circuit cell were measured prior to the addition of the RT. The theoretical total capacity of

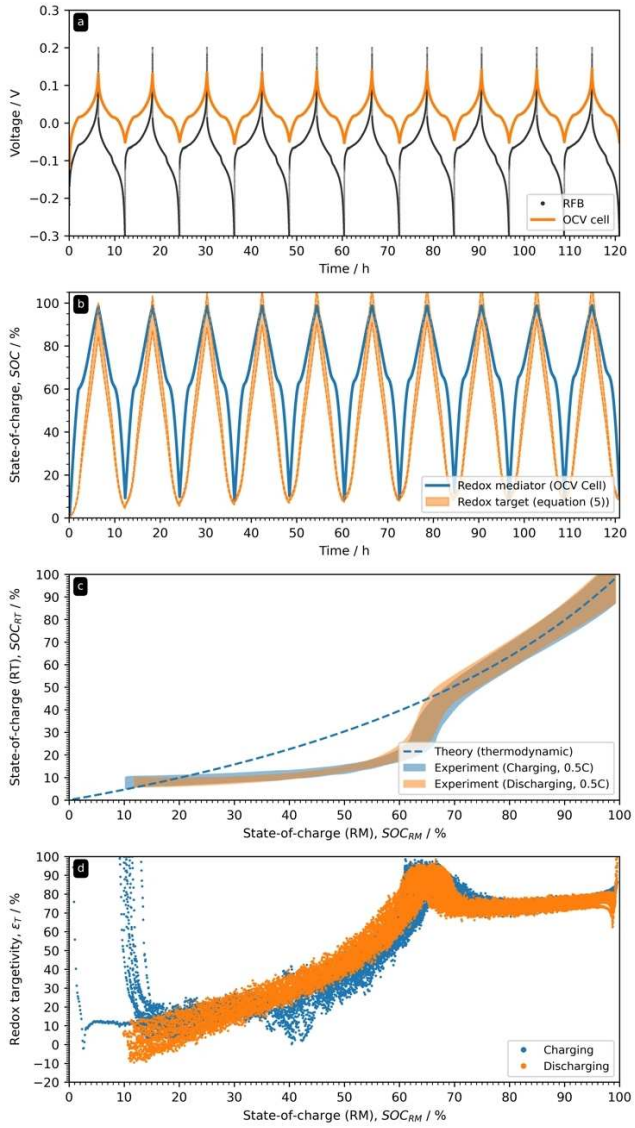

Figure 7. In-operando estimation of the redox target's SOC by monitoring the SOC of the redox mediator with a symmetric open-circuit cell. a) Open-circuit voltage for the catholyte and the voltage of the 0.1 M TEMPOAmide vs. 0.1 M TMATEMPO flow battery at 4.3 mA cm^{-2}, b) estimates for the SOC change of RM and RT, c) the state-of-charge of the RT plotted over the SOC of the RM, and d) the estimated redox targetivity of the system. SOCs of the RT are plotted as ranges showing the maximum and minimum values to account for the measurement accuracy of the degree of oxidation.

the RT (73 ± 9 mAh) was estimated from the theoretical specific capacity of the PTMAm (112.6 mAh g^{-1}), the mass of the composite material (1.5 g), the mass fraction of the PTMAm (60%) in the composite, and the degree of oxidation of the TEMPO units in the polymer (EPR: 71.8 ± 8.5%). It should be noted that a recent in-depth comparison between EPR measurements and traditional redox titration revealed that EPR tends to underestimate the actual degree of oxidation significantly.[14] The total capacity of the RT containing RFB in the first cycle was 136.2 mAh. Subtracting the total capacity of the electrolyte yields a experimental RT capacity of 85.5 mAh that represents a degree of oxidation of 84.4%. Since we do not know the true amount of the RT being charged and discharged, this value represents only a lower limit for the degree of oxidation. Hence, during the evaluation of the redox targetivity measurement, all calculations were performed assuming the lower and upper limits of the degree of oxidation (i.e., 84.4% and 100%) as well as the corresponding total capacity of the redox target [i.e., $\min(Q_{RT,t}) = 85.5$ mAh and $\max(Q_{RT,t}) = 101.3$ mAh]. Figure 7a shows an evolution of the RFB voltage and the voltage of the symmetric open-circuit cell applied for the SOC measurements. It is evident that the overall behavior of the open-circuit voltage follows expected patterns and, thus, the SOC of the RM can be readily obtained from the data. Figure 7b provides an overview of the SOC evolution for both the RM and RT over time demonstrating their in-operando accessibility.

An initial SOC of 0% was assumed for the calculations of the SOC_{RT} values. The SOC_{RT} is plotted as a range which corresponds to the aforementioned assumptions about the total capacity of the RT. It is notable that the RM does not return to 0% SOC after the first charging cycle, which can be attributed to mass-transfer limitations caused by the higher pressure drop introduced into the system by addition of the RT. Figure 7c plots the SOC data of both RT and RM over each other and represents an improved type of plot which allows for easier interpretation and a comparison with the theoretically expected behavior (dashed line) derived in our previous study.[9]

It can be clearly seen that the SOC of the RT increases slowly with a nearly linear dependency over a large portion of the charging process. At $SOC_{RM} > 50\%$ there is an increase in the rate of change of the RT's state-of-charge recognizable, which significantly speeds up for $SOC_{RM} > 60\%$ indicating a significant increase in the kinetics of the redox targeting reaction. The latter can be explained by the increasing equilibrium potentials of the RM and the RT. The difference between both potentials is the driving force for the targeting reaction. Subsequentially, the rate of change slows down again for $SOC_{RM} > 65\%$. The theoretical expectation from a thermodynamic point of view would predict a continuous increase of the RT's state-of-charge over the complete SOC range of the RM. However, the thermodynamic approximation significantly overestimates the state-of-charge of the RT for values below the threshold SOC in comparison to the empirical data. This is due to the thermodynamic prediction not taking into account any overpotentials for the redox targeting reaction. It, thus, neglects the kinetic and hydrodynamic effects within the system, which seem to govern the targeting process for values below the threshold. Interestingly, the experimental data and the thermodynamic prediction are in excellent agreement – within the bounds of measurement uncertainty – for SOC values above the threshold. This indicates that for $SOC_{RM} > 65\%$ the targeting reaction is not limited by the kinetics of the reaction anymore.

Finally, Figure 7d displays the redox targetivity calculated by Equation (10) which further supports the previous interpretation. To recapitulate, the displayed percentages represent the percentage of the total applied current that is effectively charging/discharging the RT. During the charging process, the redox targetivity increases continuously and peaks at around 95% before it stabilizes at a plateau value between 70% and

80%. The limited targetivity is a result of the competing processes of discharging the RM at the RT and re-charging the RM in the flow cell to keep up the driving force for the targeting reaction. These findings are in line with the study about the important role of kinetic effects in redox targeting reactions reported by Sevov and co-workers recently.[10]

The presented in-operando measurements of the RT's state-of-charge and the redox targetivity demonstrate the benefits and capabilities of this new measurement technique and the proposed figure-of-merit, respectively. Further methodological investigations are required, for example, to increase the accuracy of the method, to understand the impact of the various operational and physicochemical parameters of the flow battery, and to understand its yet unknown pitfalls.

Conclusion

A new combination of redox mediator and redox target has been evaluated for the use in an all-organic redox targeting flow battery. By the use of the hydrophilic poly(TEMPO-methacrylamide) (PTMAm) as the redox target, the compatibility with an aqueous redox mediator containing electrolyte was enhanced compared to the previously employed poly(TEMPO-methacrylate) (PTMA). The polymer was combined with *N*,*N*,*N*-trimethyl-2-oxo-2-[(2,2,6,6-tetramethylpiperidin-4-yloxyl)-amino]ethan-1-ammonium chloride (TEMPOAmide) as the redox mediator. By this, the redox active group of the mediator and the target are structurally very similar and exhibit similar formal redox potentials with a small difference of –21 mV in 1 M $NaCl_{aq.}$

The polymeric material was processed into water-insoluble porous granules by applying sodium alginate as a binder followed by extrusion into calcium chloride solution. After freeze-drying, a porous targeting material was obtained. This processing route is of straightforward nature and is readily adaptable to alternative water-compatible redox targeting chemistries.

From these materials, redox targeting flow batteries have been constructed that were stably operated for 100 consecutive cycles at targeting conditions. Total capacities of up to 100 mAh in galvanostatic cycling mode (8.3 mA cm^{-2}) and 131 ± 2 mAh in potentiostatic cycling mode were achieved, which is among the highest absolute capacities demonstrated for an all-organic redox targeting flow battery reported so far. Furthermore, a capacity utilization of >90% of the theoretical capacity (115 ± 10 mAh) of the battery was observed for the potentiostatic cycling mode. The rate capability of the composite granule system with the hydrophilic active material is comparable to the rate capabilities of the PTMA powder system, that was recently presented by us.[9] This indicates that efficient targeting is possible even with millimeter sized granules, when the composite particles are porous enough.

In addition to the material investigations, a new figure-of-merit – the redox targetivity – was proposed and equations were derived that enable the in-operando estimation of this quantity and the state-of-charge of the redox target from the measurable state-of-charge of the redox mediator and coulomb counting. The general working principle of this method was demonstrated experimentally in this study. Significant charging and discharging rates for the redox target (RT) occurred at redox mediator state-of-charges (SOCs) above 50% and reached a maximum redox targetivity of 95% at mediator SOCs between 60% and 70%. While a detailed methodological optimization of this approach was out of the scope of this study, it is clear from the obtained results that the in-operando estimation of the redox target's SOC and the derived redox targetivity can become a powerful tool for the investigation and optimization of redox targeting flow batteries (RTFB) in the future.

Experimental Section

Materials

SuperP was obtained by Alfa Aesar. *N*-Methylpyrrolidone (NMP) was purchased at TCI and used as obtained. Sodium alginate was obtained from Merck. Sodium chloride was obtained at Fisher Chemical.

Synthesis

The redox mediator *N*,*N*,*N*-trimethyl-2-oxo-2-[(2,2,6,6-tetramethyl-piperidin-4-yloxyl)amino]ethan-1-ammonium chloride (TEMPOA-mide) was synthesized according to a procedure recently published by our group.[14] The polymer poly(2,2,6,6-tetramethylpiperdinyloxy-4-yl-methacrylamide) (PTMAm) was synthesized according to our recent publication.[12] It exhibited a degree of oxidation of 71.8 ± 8.5% (EPR). The measurement uncertainty was estimated from three-fold repetition of the sample preparation and measurement.

Alginate bound composite

For the aqueous processing, PTMAm (2 g) was mixed with SuperP (1.168 g). To this, 28 mL of a stock solution of sodium alginate (420 mg in 70 mL of water) was added and the mixture was homogenized and left to swell overnight. The mixture was then stirred at 4000 rpm with a blade stirrer, casted into a petri dish, and dried at 70 °C in the oven. Afterwards, the solid was transferred into an aluminium oxide mortar and ground finely.

For the first high-capacity approach, the composite (1.511 g) was transferred into a 20 mL syringe, 7.8 mL of water was added, and the mixture was shaken and swollen for 1 h. The content of the syringe was then pushed slowly into a 1 M $CaCl_2$ solution in water. The composite "worms" were consequently collected on a frit, frozen in liquid nitrogen and lyophilized overnight. The dried material was then cut in 2 mm granules and used as battery composite.

Cyclic voltammetry

For cyclic voltammetry (CV), a three-electrode setup was utilized with a glassy carbon working electrode (BioLogic, 4.8 mm diameter), Ag/AgCl reference electrode (BioLogic), and Pt-wire counter electrode. For the redox potential determination of the redox mediator, standard CV measurements were performed at 10 mV s^{-1}. For the measurement of the redox target standard potential, a small electrode disc was punched out of the casted electrode sheets and added to the top of a glassy carbon electrode. This was done by fixing the glassy carbon electrode in a cut-off syringe with

carbon felt at its tip, that is in contact to the backside of the small (2 mm) electrode disc.

For the CV of the redox targeting pair, the setup presented previously by our group and Zhou et al. was utilized.[8,9] A polymer composite layer sample was cut out and added to a sample tray that can be filled with electrolyte. From the top, an either 10 mM TEMOPOAmide solution in 1 M NaCl or pure 1 M NaCl aqueous solution-soaked separator (Kimtech tissue) was added. The separator was then contacted directly with the working electrode from above. The rest of the sample tray could be filled with either 1 M NaCl or 1 M NaCl with 10 mM of RM. The same setup was also used in the absence of the solid composite. CVs were measured at 2 $mV\,s^{-1}$ scanning speed. If the target is separated from the working electrode and no mediator is present, no CV signal was obtained. If no composite is present, but the tray is filled with RM solution, the standard CV shape for the RM was obtained. When the RT composite was added, the CV signal changed into a sigmoidal shape indicating diffusion-limited redox behaviour.

Flow battery testing

For the battery cycling experiments, flow battery cells were constructed using a Fumasep FAA-3-50 anion exchange membrane. Generally, the battery materials were tested in a compositionally symmetric and unbalanced flow battery. However, to reduce the required amount of TEMPOAmide, *N,N*-2,2,6,6-heptamethylpiperidinyloxy-4-ammonium chloride (TMATEMPO) was utilized as non-capacity limiting side (NCLS). The TMATEMPO was charged in 1.066 M concentration in 1 M $NaCl_{aq}$ vs. dimethylviologen. This solution was subsequently diluted with an uncharged solution of the same concentration to obtain a 50% SOC solution. Dilution with $NaCl_{aq}$ yielded lower concentrations of 10 mM and 100 mM of 50% SOC. Typically a 20-fold excess was used for the NCLS. For the capacity-limiting side (CLS), the TEMPOAmide material was charged vs. dimethylviolgen in 100 mM concentration in 1 M $NaCl_{aq}$. This solution was then diluted with an uncharged TEMPOAmide solution of the same concentration and 1 M $NaCl_{aq}$ to obtain a 50% SOC solution of 10 mM concentration. For the 100 mM concentration test, the TEMPOAmide material was used in 0% SOC as CLS and TMATEMPO was used in 50% SOC as NCLS. For the standard tests, 16 mL of CLS and 320 mL of NCLS were utilized.

Initially the cells were cycled at 0.86, 1.72, 4.3, 8.6 and 17.2 $mA\,cm^{-2}$ (10 mm) or 8.6, 4.3, 17.2, 43.0 $mA\,cm^{-2}$ (100 mm) before the redox target cartridge was added to the electrolyte circuit. For this a standard liquid chromatography cartridge is used, that was fitted with a graphite felt filter on the bottom. 150 mg (10 mm) or approximately 1.5 g (100 mm) redox target composite was added to the cartridge and the battery cycling was repeated. Also, potentiostatic charging was performed after the rate testing. After these cycles, a cartridge with the redox targeting material was introduced into the pumping circuit.

EPR measurements

X-band EPR spectra were acquired on an EMXmicro CW-EPR spectrometer from Bruker, Germany. The SpinCountQ software module was used for the determination of the spin count. A known PTMA polymer (radical content of 80%, determined through redox titration) was used as a reference. The radical contents of the TEMPO-containing compounds were determined from the mean values derived from the EPR spectra of three samples per compound.

Author Contributions

E.S.: Conceptualization (equal), methodology (supporting), investigation (lead), data curation (equal), formal analysis (equal), visualization (lead), writing – original draft (equal), and writing – review and editing: critical review (equal). C.S.: conceptualization (equal), methodology (lead), investigation (supporting), data curation (equal), formal analysis (equal), visualization (supporting), writing – original draft (equal), writing – review and editing: critical review (equal), and supervision of E.S. (equal). J.M.: Investigation (supporting) and writing – review and editing: critical review (equal). M.D.H.: writing – review and editing: critical review (equal), supervision of E.S. (equal), and funding acquisition (equal). U.S.S.: writing – review and editing: critical review (equal), supervision of E.S. (equal), and funding acquisition (equal).

Acknowledgements

We thank Steffi Stumpf for the measurements of the SEM images. The SEM facilities of the Jena Center for Soft Matter (JCSM) were established with a grant from the German Research Foundation (DFG). Open Access funding enabled and organized by Projekt DEAL.

Conflict of Interests

The authors declare no conflict of interest.

Data Availability Statement

The data that support the findings of this study are available from the corresponding author upon reasonable request.

Keywords: redox targeting · redox flow battery · capacity enhancement · polymer batteries · aqueous batteries

[1] E. Sánchez-Díez, E. Ventosa, M. Guarnieri, A. Trovò, C. Flox, R. Marcilla, F. Soavi, P. Mazur, E. Aranzabe, R. Ferret, *J. Power Sources* **2021**, *481*, 228804.
[2] A. Lucas, S. Chondrogiannis, *Int. J. Electr. Power Energy Syst.* **2016**, *80*, 26.
[3] J. Winsberg, T. Hagemann, T. Janoschka, M. D. Hager, U. S. Schubert, *Angew. Chem. Int. Ed.* **2017**, *56*, 686.
[4] a) P. Arévalo-Cid, P. Dias, A. Mendes, J. Azevedo, *Sustain. Energy Fuels* **2021**, *5*, 5366; b) I. Iwakiri, T. Antunes, H. Almeida, J. P. Sousa, R. B. Figueira, A. Mendes, *Energies* **2021**, *14*, 5643.
[5] a) F. Zhang, M. Gao, S. Huang, H. Zhang, X. Wang, L. Liu, M. Han, Q. Wang, *Adv. Mater.* **2021**, e2104562; b) X. Wang, J. Chai, J. Jiang, *Nano Mater. Sci.* **2021**, *3*, 17; c) J. Ye, L. Xia, C. Wu, M. Ding, C. Jia, Q. Wang, *J. Phys. D* **2019**, *52*, 443001; d) S. Mubeen, Y.-S. Jun, J. Lee, E. W. McFarland, *ACS Appl. Mater. Interfaces* **2016**, *8*, 1759; e) V. M. Ortiz-Martínez, L. Gómez-Coma, G. Pérez, A. Ortiz, I. Ortiz, *Sep. Purif. Technol.* **2020**, *252*, 117436.
[6] C. M. Wong, C. S. Sevov, *ACS Energy Lett.* **2021**, *6*, 1271.
[7] M. Zhou, Q. Huang, T. N. Pham Truong, J. Ghilane, Y. G. Zhu, C. Jia, R. Yan, L. Fan, H. Randriamahazaka, Q. Wang, *Chem* **2017**, *3*, 1036.

[8] M. Zhou, Y. Chen, M. Salla, H. Zhang, X. Wang, S. R. Mothe, Q. Wang, *Angew. Chem. Int. Ed.* **2020**, *59*, 14286.
[9] E. Schröter, C. Stolze, A. Saal, K. Schreyer, M. D. Hager, U. S. Schubert, *ACS Appl. Mater. Interfaces* **2022**, *14*, 6638.
[10] G. Lee, C. M. Wong, C. S. Sevov, *ACS Energy Lett.* **2022**, *7*, 3337.
[11] a) H. Zhang, Q. Huang, X. Xia, Y. Shi, Y.-M. Shen, J. Xu, Z. Chen, J. Cao, *J. Mater. Chem. A* **2022**, *10*, 6740; b) D. Kim, M. S. Sanford, T. P. Vaid, A. J. McNeil, *Chem. Eur. J.* **2022**, *28*, e202200149.
[12] E. Schröter, L. Elbinger, M. Mignon, C. Friebe, J. C. Brendel, M. D. Hager, U. S. Schubert, *J. Power Sources* **2023**, *556*, 232293.
[13] a) K. Koshika, N. Sano, K. Oyaizu, H. Nishide, *Macromol. Chem. Phys.* **2009**, *210*, 1989; b) K. Koshika, M. Kitajima, K. Oyaizu, H. Nishide, *Green Chem. Lett. Rev.* **2009**, *2*, 169.
[14] P. Rohland, O. Nolte, K. Schreyer, H. Görls, M. D. Hager, U. S. Schubert, *Mater Adv* **2022**, *3*, 4278–4288.
[15] M. Moghaddam, S. Sepp, C. Wiberg, A. Bertei, A. Rucci, P. Peljo, *Molecules* **2021**, *26*, 2111.
[16] O. Nolte, I. A. Volodin, C. Stolze, M. D. Hager, U. S. Schubert, *Mater. Horiz.* **2021**, *8*, 1866.
[17] Y. Ding, X. Zhong, C. Yuan, L. Duan, L. Zhang, Z. Wang, C. Wang, F. Shi, *ACS Appl. Mater. Interfaces* **2021**, *13*, 20681.
[18] G. T. Grant, E. R. Morris, D. A. Rees, P. J. Smith, D. Thom, *FEBS Lett.* **1973**, *32*, 195.
[19] C. Stolze, M. D. Hager, U. S. Schubert, *J. Power Sources* **2019**, *423*, 60.

Manuscript received: February 27, 2023
Revised manuscript received: March 24, 2023
Accepted manuscript online: April 4, 2023
Version of record online: April 4, 2023